A novel bis-1,2,4-benzothiadiazine pincer ligand: Synthesis, characterization and its first row transition metal complexes

Konstantina Pringouri, Muhammad U. Anwar*, Liz Mansour, Nathan Doupnik, Yassine Beldjoudi, Emma L. Gavey, Melanie Pilkington, and Jeremy M. Rawson*

Supplementary Information

Crystallographic Details

Additional Crystallographic Details

Complex **1** exhibited rotational disorder of both the CF_3 and SO_3 groups of the triflate counterion which was modelled over two sites in a 1:1 ratio with common U_{iso}.

For complex **2** two acetonitrile molecules were located, one of which was part occupancy. The *sof* of the partial occupancy was refined against the full-occupancy MeCN using a common U_{iso} for chemically equivalent atoms. Attempts to refine the MeCN anisotropically led to distorted ellipsoids indicating potential disorder in MeCN positions. The solvent was refined isotropically given the poor data: parameter ratio. Residual diffuse electron density appeared associated with a disordered solvent molecule which was modelled as an O atom (H_2O) over 5 sites until the residual electron density was less than 1 e^-/A^3. In the latter stages of refinement, a 2-component inversion twin was included to accommodate a slight twinning based on the Flack parameter (< 0.05).

Both BF_4^- anions in complex **3** showed some disorder; one BF_4^- *via* a rotation about two F atoms which are H-bonded to N-H groups and the second one *via* translational disorder reflected in elongated U_{ij} in the same direction for all five atoms. The former was modelled over two sites using common U_{iso} to identify *sof*'s and then the *sof* were fixed and and U_{ij} refined anisotropically. The second BF_4^- was modelled isotropically over three sites with common U_{iso} in a 0.25:0.25:0.50 ratio. Two MeCN molecules were identified and refined with 1,2- and 1,3-DFIX commands to maintain a linear geometry. One MeCN was disordered over two sites *via* a pivoting motion about the terminal N atom. Two part occupancy O atoms were located in the vicinity of a ligand N-H group - subsequent anisotropic refinement led to further splitting and in latter cycles of least squares the O was refined isotropically over 4 positions with common U_{iso}. Residual remaining electron density was treated with SQUEEZE. Although the final *R* values remained relatively high, the connectivity of the cationic complex and the two BF_4^- anions were clearly defined.

For complex **5**, H atoms were added at calculated positions except N-H and H-bonded O-H groups of MeOH solvate which were located in the difference map and refined with a common U_{iso} and DFIX restraints. One of the four MeOH solvent molecules was not H-bonded and poorly defined within the structure. This was refined isotropically over three sites using common U_{iso} for C and O atoms to afford *sof*'s of 0.27, 0.37 and 0.37 respectively and led to residual electron density less than 1e^- in the vicinity of this solvent molecule. Complex **6** exhibited disorder in one triflate anion which was modelled over two sites in a 50:50 ratio with appropriate geometric constraints for CF_3 and SO_3 units. For complex **7**, hydrogen atoms were added at calculated positions except N-H protons which were located in the difference map and refined freely with common U_{iso}.

Table S1 Relative energies of the isomers of **L**H_2 computed using density functional theory (DFT) calculations with the dispersion-corrected B3LYP-D3 functional and 6-311G*$^{+}$ basis set.

	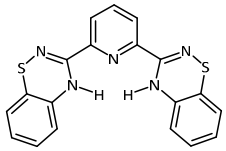	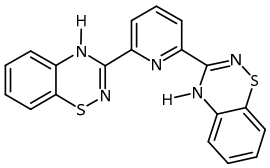	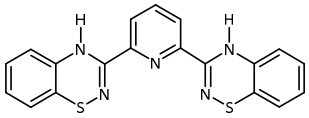
Energy/kJ/mol	0	27	81
Torsion angle/°	-7.3/3.65	2.95/-138.97	-128.84/136.59

Table S2 Selected bond lengths and angles for complexes **1** – **7**.

	M-N_{py}/Å	M-N_{BTDA}/Å	$N_{py}MN_{BTDA}$/°[a]	$N_{py}MN_{BTDA}$/°[b]	$N_{BTDA}MN_{BTDA}$/°	$N_{py}MN_{py}$/°
Mn (**1**)	2.276(2)	2.201(2)	71.00(8)	103.55(8)	86.05(8)	171.23(12)
	2.297(2)		72.22(8)	113.50(8)	104.77(12)	
					106.62(12)	
					142.96(8)	
Fe (**2**)	1.864(5)	1.969(5)	79.9(2)	98.7(2)	91.2(2)	178.6(2)
	1.888(5)	1.969(5)	79.9(2)	101.4(2)	91.6(2)	
		1.973(5)	80.0(2)	99.3(2)	91.7(2)	
		1.975(5)	80.1(2)	100.7(2)	92.4(2)	
					159.9(2)	
					159.9(2)	
Fe (**3**)	1.881(4)	1.962(5)	79.63(19)	98.20(17)	89.48(19)	178.47(17)
		1.967(5)	79.80(18)	99.95(19)	90.21(19)	
		1.970(4)	80.29(17)	100.04(19)	93.04(19)	
		1.976(4)	80.36(19)	101.71(17)	94.15(19)	
					160.0(2)	
					160.09(19)	
Co (**4**)	2.046(3)	2.128(3)	74.93(10)	93.94(10)	90.38(11)	163.82(11)
	2.059(3)	2.139(3)	75.04(10)	94.45(10)	92.28(11)	
		2.144(3)	75.51(11)	116.43(11)	93.94(11)	
		2.157(3)	75.61(10)	117.39(11)	99.90(11)	
					147.63(11)	
					149.37(11)	
Ni (**5**)	1.985(2)	2.080(2)	77.16(10)	93.16(10)	91.85(10)	177.98(10)
	1.987(2)	2.081(2)	77.29(10)	93.32(9)	92.66(9)	
		2.083(2)	77.41(9)	100.85(9)	93.16(10)	
		2.094(2)	77.53(9)	104.57(10)	93.32(9)	
					154.57(10)	
					154.82(9)	
Zn (**6**)	2.054(3)	2.165(3)	75.35(11)	73.63(11)	80.69(11)	174.64(17)
	2.055(3)	2.266(3)	103.87(11)	73.98(11)	105.11(16)	176.37(17)
		2.209(3)	75.39(11)	106.94(11)	110.12(16)	
		2.312(3)	103.17(11)	107.81(11)	149.12(11)	
					78.85(11)	
					109.38(15)	
					109.92(16)	
					149.00(10)	
Cu (**7**)[c]	1.9294(19)	2.041(2)	79.33(8)	-	157.77(8)	-
		2.0505(19)	79.36(8)			

[a] Angle within the chelate ring. [b] Angles between N atoms in different rings. [c] Cu-O/Å = 1.9298(16)-2.651(2), O-Cu-O/° = 53.95(7)-153.68(6), O-Cu-N/° = 86.83(7)-173.05(7).

Table S3 Density functional theory (DFT) single point energy calculations of the relative energies of the ligand conformations in the metal complexes using the dispersion-corrected B3LYP-D3 functional and 6-311G** basis set.

Complex	Mn (**1**)	Fe (**2**)	Zn (**6**)
	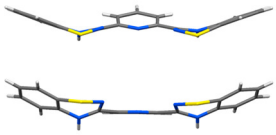		
Energy/kJ/mol	0	46	18

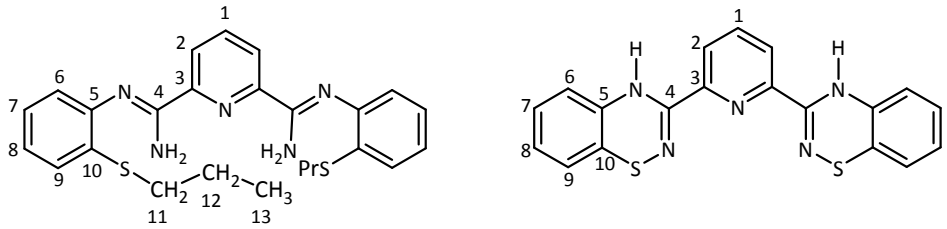

Fig. S1 Numbering scheme of bis(2-(propylthio)phenyl)pyridine-2,6-bis(carboximidamide) (left) and **L**H_2 (right).

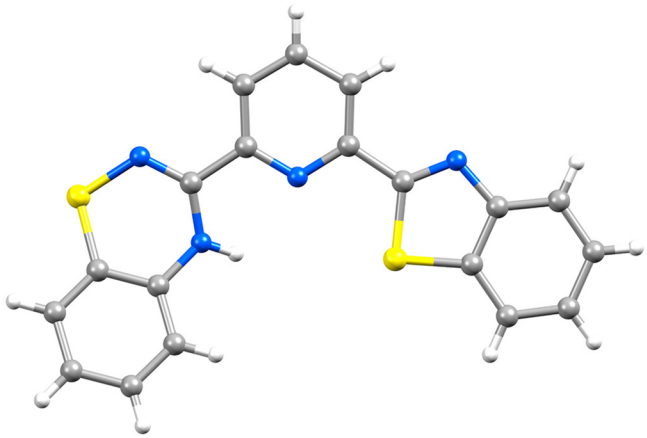

Fig. S2 Molecular structure of the by-product of the ligand (**8**).

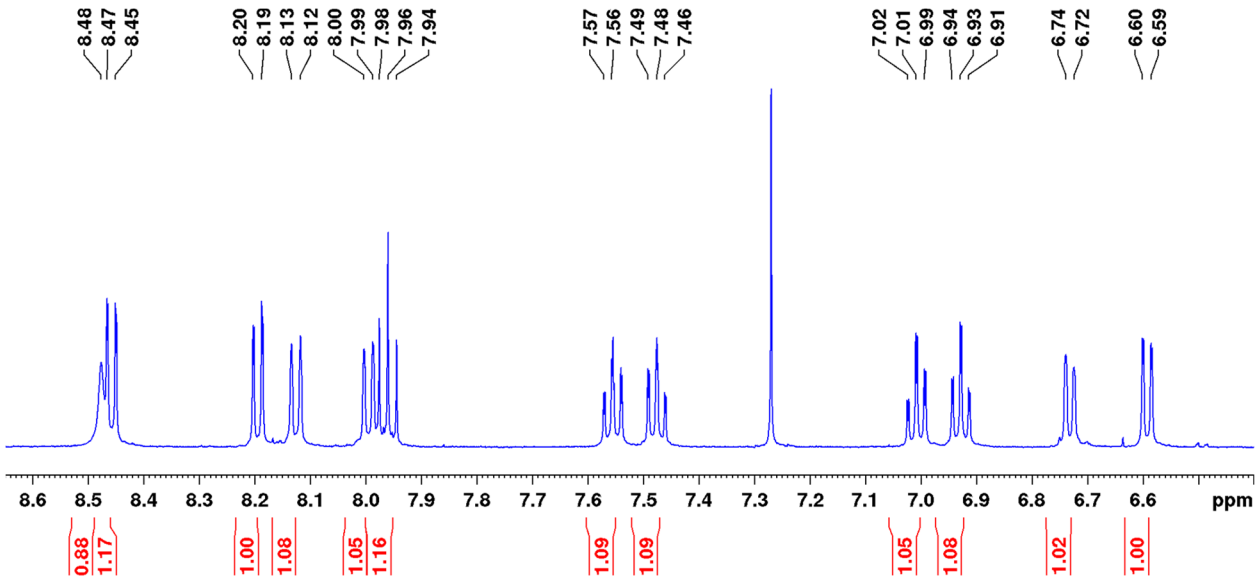

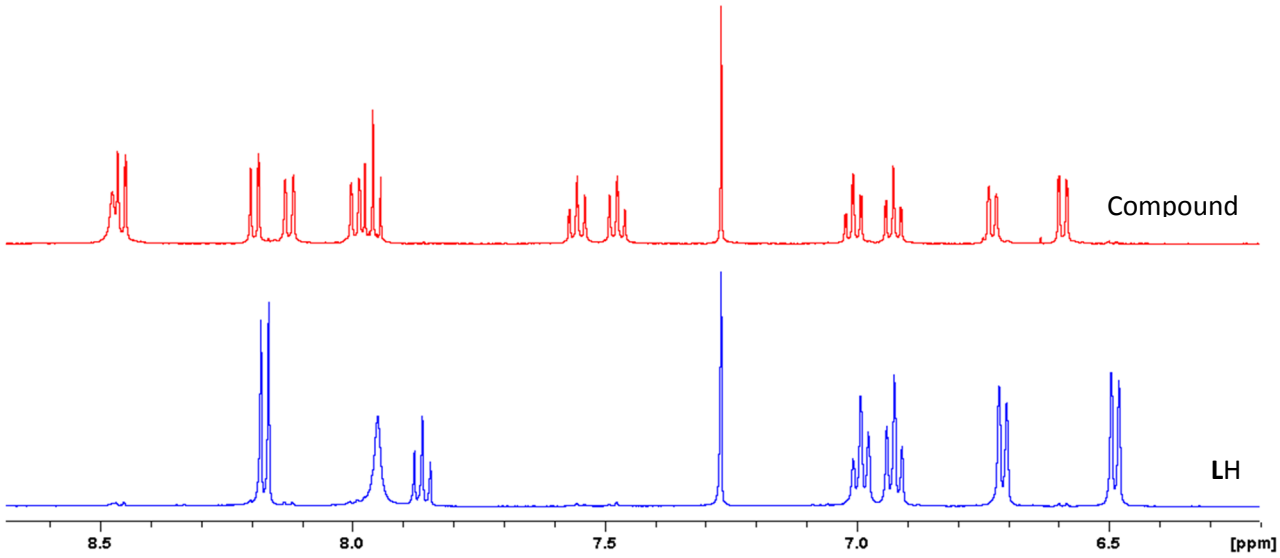

Fig. S3 ^{1}H NMR of the ligand **8** in $CDCl_3$ (top) and comparison of the ligand **L**H_2 (blue) and the decomposed product **8** (red) (bottom).

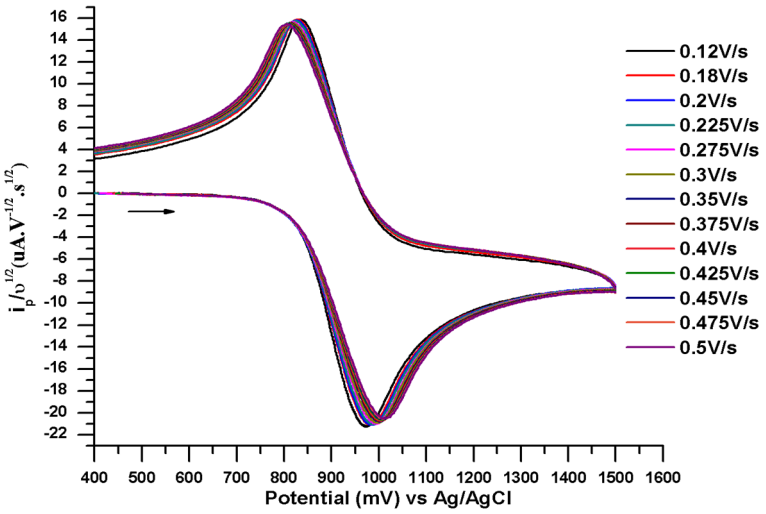

Fig. S4 Normalized cyclic voltammograms of ligand **L**H_2 (C_0 = 5.96 mmol·L^{-1}) in a solution of TBA(PF_6) in dichloromethane (0.047 mol·L^{-1}).

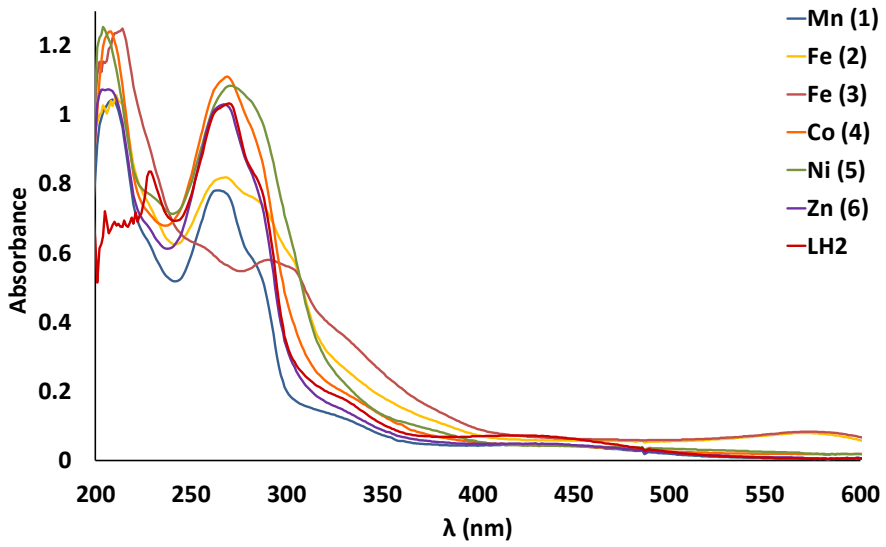

Fig. S5 Solution UV-Vis spectra of complexes **1**-**6** as well as ligand **L**H_2 to emphasize the ligand-based nature of the spectroscopic properties.

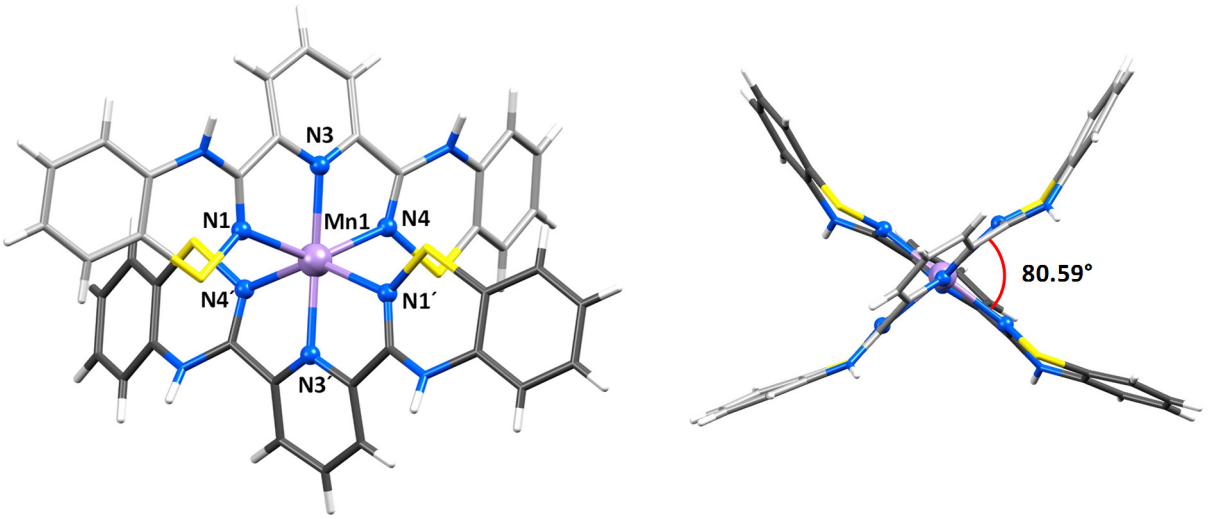

Fig. S6 Molecular structure and side-view of complexes of [Mn(**L**H_2)$_2$] (**1**). (solvent molecules and counter-ions omitted for clarity).

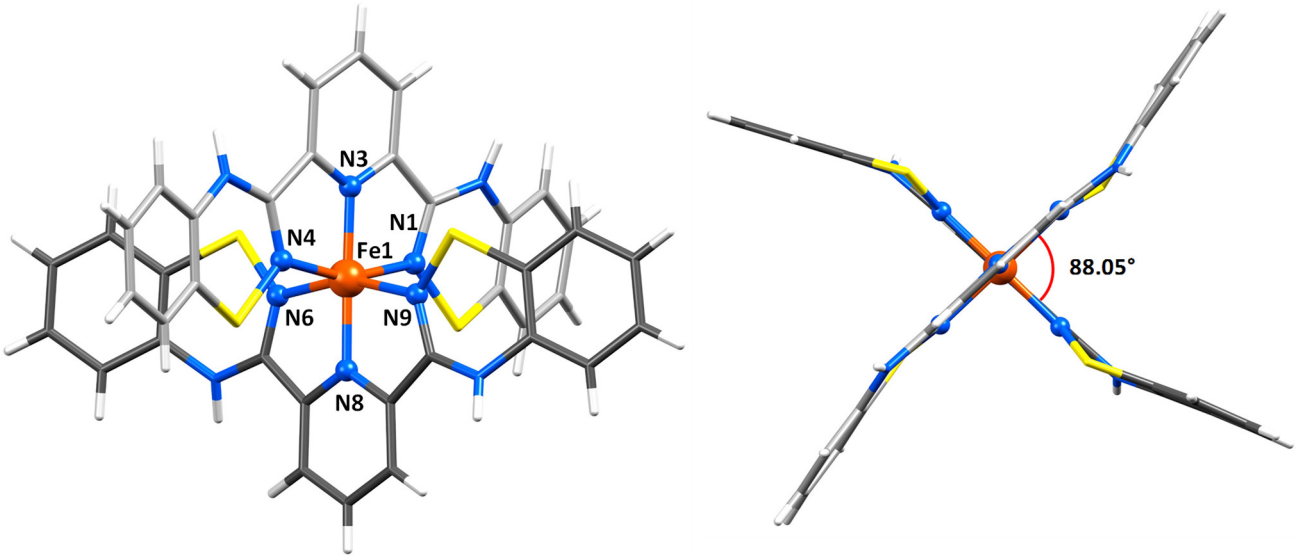

Fig. S7 Molecular structure and side-view of complexes of [Fe(**L**H_2)$_2$] (**3**). (solvent molecules and counter-ions omitted for clarity).

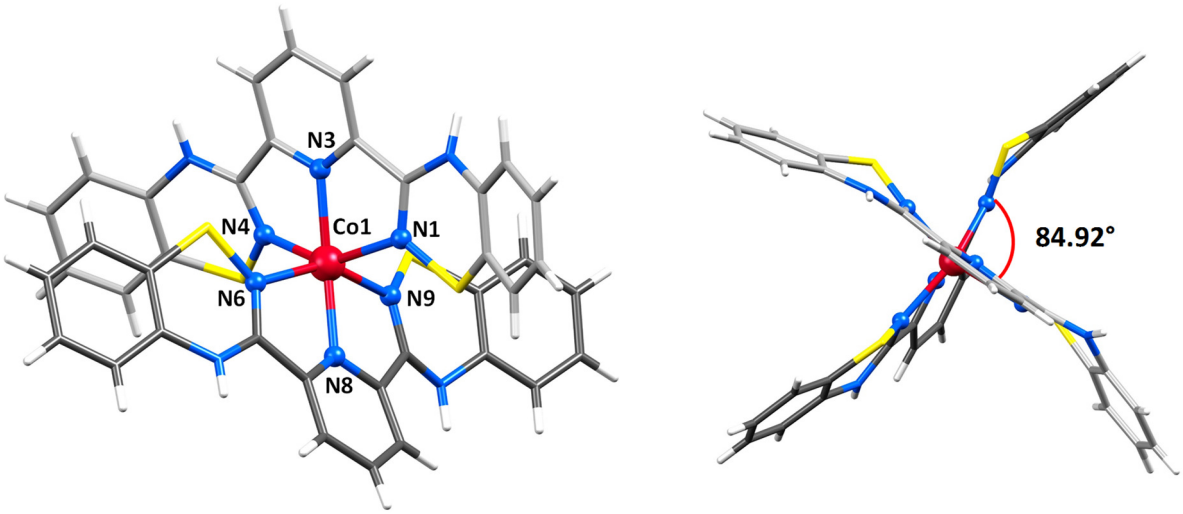

Fig. S8 Molecular structure and side-view of complexes of [Co(**L**H_2)$_2$] (**4**). (solvent molecules and counter-ions omitted for clarity).

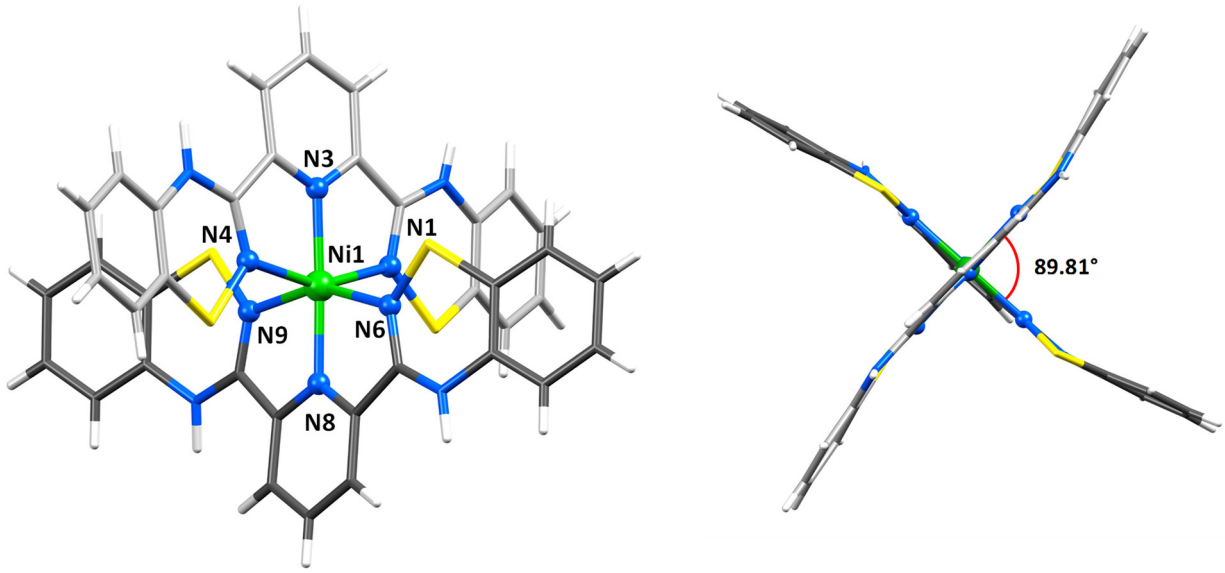

Fig. S9 Molecular structure and side-view of complexes of [Ni(**L**H_2)$_2$] (**5**). (solvent molecules and counter-ions omitted for clarity).

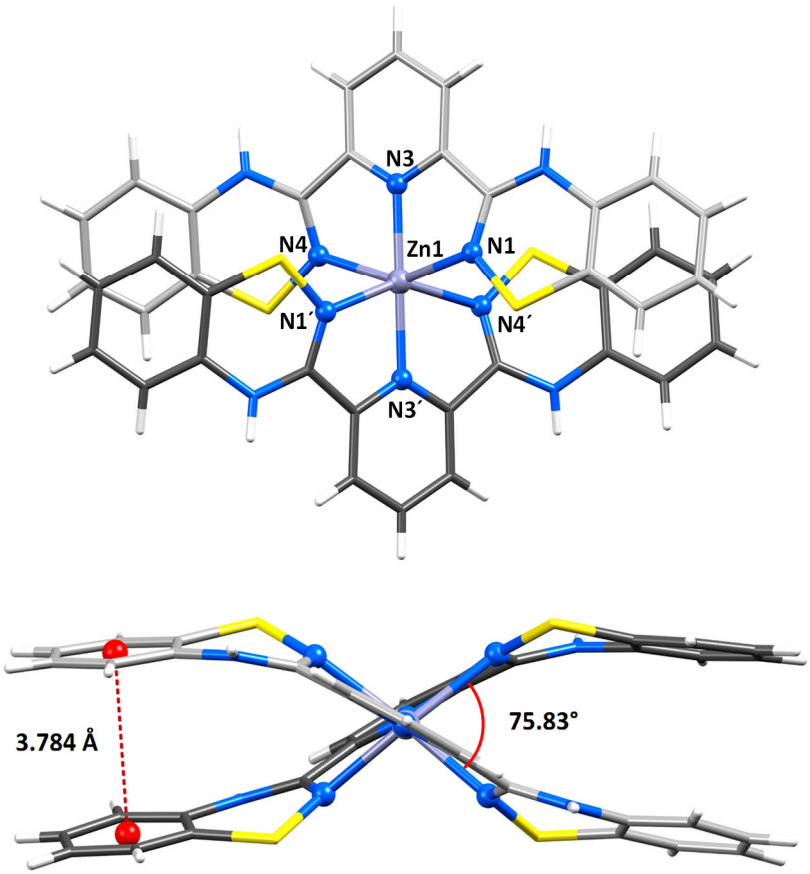

Fig. S10 Molecular structure and side-view of complexes of [Zn(**L**H_2)$_2$] (**6**). (solvent molecules and counter-ions omitted for clarity).

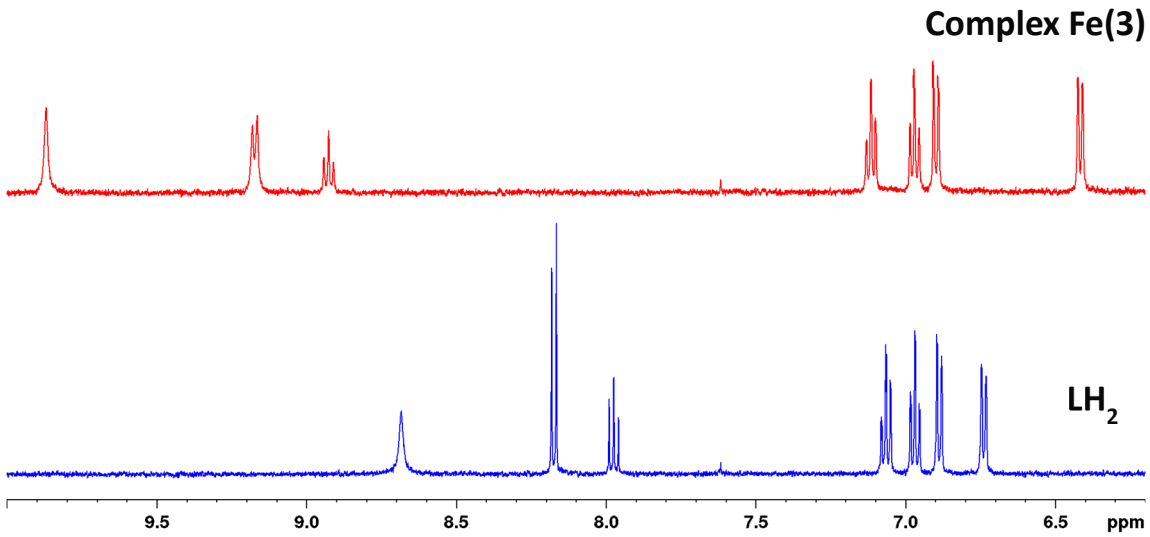

Fig. S11 ^{1}H NMR of complex **3** (top) and **L**H_2 (bottom).

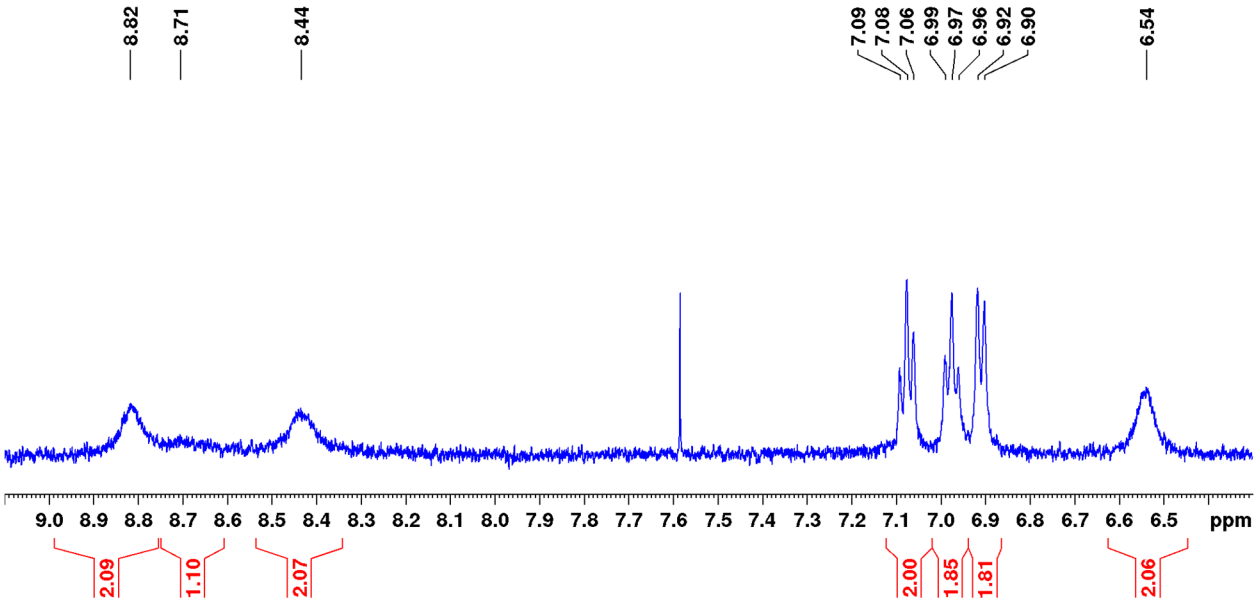

Fig. S12 ^{1}H NMR of complex **6** (d_3-MeCN).

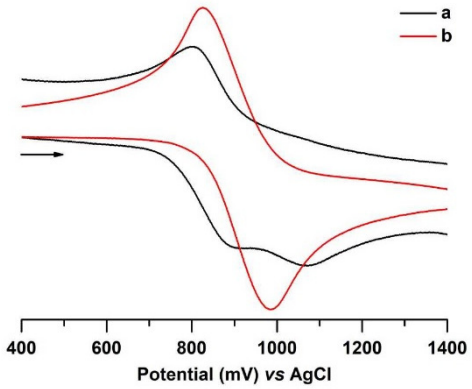

Fig. S13 Cyclic voltammogram of complex **2** (black) and **L**H_2 (red) in dichloromethane (0.047 mol·L^{-1}) with [^{n}Bu$_4$N][PF_6] supporting electrolyte at a scan rate of 0.2 V/s.

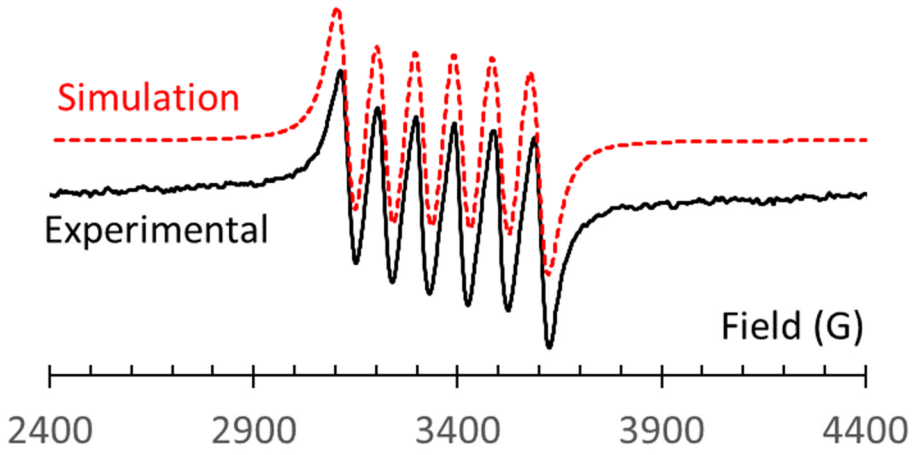

Fig. S14. Room temperature solution X-band EPR spectrum of $[Mn(\mathbf{L}H_2)_2][CF_3SO_3]_2$ in THF (g = 1.998). Simulation a_{Mn} = 94.2 G, line width = 42.3 G_{pp}.

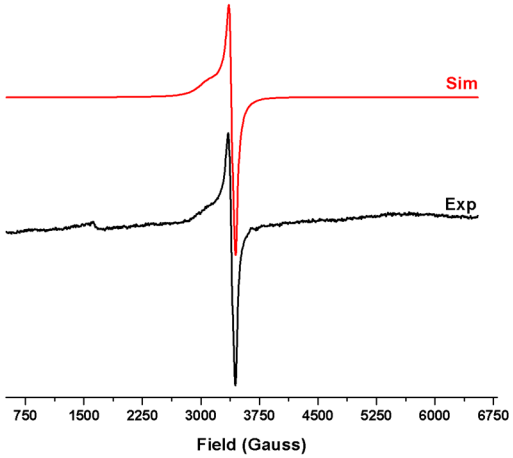

Fig. S15. Room temperature solid state EPR spectrum of $Cu(\mathbf{L}H_2)(NO_3)_2$ [Simulation: g_x = 2.29, g_y = 2.07, g_z = 2.65, a_{Cux} = 10G, a_{Cuy} = a_{Cuz} = 20G, ΔH_x = 190 G, ΔH_y = 35 G, ΔH_z = 25 G].

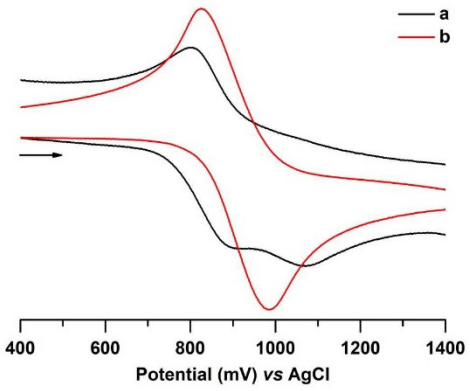

Fig. S16. Cyclic voltammogram of **2** (black, a) and **L**H_2 (red, b) in dichloromethane (0.047 mol·L^{-1}) with [^{n}Bu_4N][PF_6] supporting electrolyte at a scan rate of 0.2 V/s.